Pinpointing Element Transfer Locations during Submerged Arc Welding

Element transfer locations were revealed through quantification of transfer levels from CaO-SiO_2-MnO-TiO_2 fluxes to droplets and the weld metal

BY G. WANG, Y. ZHANG, H. TIAN, Z. LI, AND C. WANG

Abstract

Due to the shielding effect of fluxes, investigations into element transfer during submerged arc welding are often restricted by and/or limited to compositional analysis of the weld metal (WM). Therefore, meaningful discussions about specific locations where responsible reactions occur, such as the arc-containing droplet zone and arc-free slag-metal zone, are often nebulous. To counter such challenges, designed droplet collection trials were conducted over a water-cooling system. By examining the contribution of droplets to element transfer in the WM, the locations and possible pathways facilitating salient element transfer behaviors were elucidated. The results indicated that the transfer levels of Si, Mn, and Ti from the flux into the droplet were, on average, 0.016 wt-%, 0.079 wt-%, and 0.004 wt-% higher, respectively, than levels into the WM, suggesting that element transfer occurred primarily in the droplet zone. The transfer level of O from fluxes into droplets was, on average, 0.022 wt-% lower than that to the WM, indicating that beyond the droplet zone, alternative sources contributed to the increase in O content within the WM. The findings provide a theoretical foundation for precisely manipulating WM compositions and potentially optimizing the entire welding process to a new level.

Keywords

- Submerged Arc Welding
- Droplet Zone
- Element Transfer
- Flux
- Weld Metal

Introduction

Numerous studies into submerged arc welding (SAW) have emphasized that tuning compositions of the weld metal (WM) is crucial for yielding a weld joint with satisfactory toughness (Refs. 1–4). For instance, increasing Mn and Si contents in the WM contributes to solid solution strengthening. At the same time, Si also inhibits carbide precipitation, enhancing both the strength and toughness of the weld joint (Refs. 5–7). Additionally, elevated Ti content facilitates the formation of Ti-containing nano-scale inclusions and, thus, promotes the development of acicular ferrite in the WM, thereby improving resistance to cold cracking of the end-user product (Ref. 8).

Previous studies have predominantly focused on compositional analysis of the WM, yet consensus regarding the exact locations of element transfer has not been reached (Refs. 9, 10). Mitra et al. (Ref. 11) and Zhang et al. (Ref. 12) suggested that transfer of Si and Mn occurred via a slag-metal interface in the reaction zone. Conversely, Kim et al. (Ref. 13) proposed that alloying elements were mainly transferred into the droplets via electrochemical and thermochemical reactions in the droplet zone. Variations in physical and chemical properties, such as mass, electronegativity, and ionization energy, result in distinct behaviors among elements in response to electromagnetic forces, reactivity with various substances, and ionization tendencies (Ref. 14). Additionally, in the arc plasma-containing zone, the presence of high-energy electrons and ions facilitates the ionization and excitation of substances. In contrast, in the non-arc zone, reactions are primarily governed by thermodynamic equi-

https://doi.org/10.29391/2026.105.002

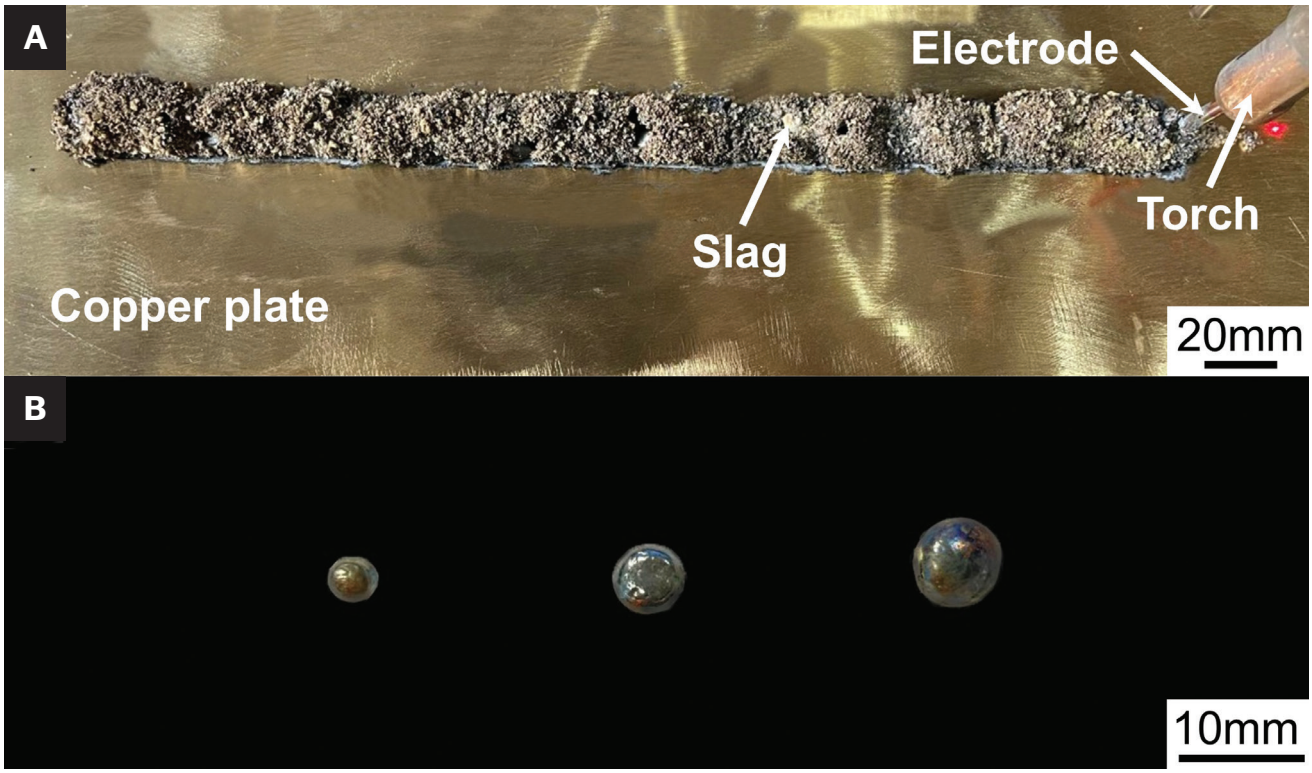

Fig. 1 — Macrographs of: A — Droplet collection experiment; B — typical droplets.

librium (Ref. 15). Neglecting these differences may lead to discrepancies between flux design or process optimization and actual element transfer conditions, negating precise control and diminishing production efficiency. Consequently, it is essential to ascertain the specific locations of element transfer by fully elucidating element transfer behaviors within each specific reaction zone.

However, the shielding effect incurred by fluxes poses significant challenges for determining the precise locations of element transfer (Ref. 16). To isolate the reaction results within the droplet zone during SAW, Wang et al. (Ref. 17) performed a droplet collection experiment utilizing an apparatus designed for capturing droplets with CaO-SiO_2-MnO fluxes. Their findings indicated that increased welding current and MnO content in the fluxes enhanced element transfer levels within the droplet zone. Furthermore, Tathgir et al. (Ref. 18) believed that the ionization products of TiO_2 contributed to an increased energy density of the arc by constricting the arc column, suggesting that it could similarly promote Mn transfer without necessitating excessive increases in current. Moreover, incorporating TiO_2 into CaO-SiO_2-MnO fluxes can modulate the oxygen potential of fluxes, thereby mitigating O content in the WM. Nevertheless, elucidating element transfer behavior solely within the droplet zone is insufficient for determining the specific locations of element transfer during SAW. Building upon prior findings, the present study further quantifies the transfer levels of elements from fluxes into droplets and WM, respectively. The former denotes the contribution of droplets to the WM composition, while the latter represents the total quantity of elements transferred to the WM. Therefore, by comparing these two transfer levels, the element transfer behavior beyond the droplet zone can be identified, providing insight into the dynamic behavior of element transfer during SAW.

In this study, CaO-SiO_2-MnO-TiO_2 fluxes were employed for droplet collection and SAW experiments. The element transfer levels between droplets and WM were quantified and compared, and the contribution of the arc and non-arc zone to element transfer during SAW was elucidated, thereby clarifying the underlying location. Determining element transfer locations and dynamic behaviors clarifies key control factors during SAW and addresses gaps in understanding element transfer. By elucidating the contributions of different zones to element transfer, this research guides flux optimization, improves the utilization efficiency of target oxides, and reduces production costs. By quantifying the contribution of each stage to element transfer in the fluxes-droplet-weld pool-WM process, flux design can be systematically optimized to minimize unnecessary oxidation losses and element burnout, thereby enhancing the effective utilization of alloying elements. Furthermore, elucidating the transfer pathways and behavioral characteristics of oxides during SAW will facilitate improvements in flux reusability and provide a scientific foundation and optimization strategy for flux recycling.

Experimental

As for the flux design, the TiO_2 content was varied from 0 to 25 wt-%, with CaO and SiO_2 content being fixed at 20 wt-% and 30 wt-%, respectively, and MnO making up the

Table 1 — Chemical Compositions of Employed Welding Fluxes (wt–%)

Fluxes No.	CaO	SiO_2	MnO	TiO_2	T_{lq}(K)
F-1 Designed	20	30	50	0	1555
F-1 Measured	19.78	29.84	50.38	0.00	
F-2 Designed	20	30	45	5	1542
F-2 Measured	19.58	29.73	45.48	5.21	
F-3 Designed	20	30	40	10	1597
F-3 Measured	19.43	29.82	40.66	10.09	
F-4 Designed	20	30	35	15	1612
F-4 Measured	19.72	29.87	35.24	15.17	
F-5 Designed	20	30	30	20	1607
F-5 Measured	19.37	29.76	30.46	20.41	
F-6 Designed	20	30	25	25	1589
F-6 Measured	19.64	29.61	25.59	25.16	

Table 2 — Chemical Compositions of Employed Base Metal and Electrode (wt-%)

Sample	C	Si	Mn	Ti	Cu	O	P	S
Base Metal	0.120	0.137	1.500	0.011	0.020	0	0.015	0.001
Electrode	0.080	0.019	1.639	0	0.021	0.008	0.013	0.016

remainder. The flux composition dictates that the melting temperature of the fluxes is 100–300 K lower than that of the base metal (BM). The mass ratio of CaO/SiO_2 was consistently upheld at a constant value to attain advantageous melting points, approximately at 1573 K, and to ensure the requisite impact toughness of the WM (Refs. 19, 20). The chemical compositions and corresponding melting points of the fluxes are given in Table 1.

Each 1 kg of reagent powder underwent 30 min of thorough mixing in a three-dimensional mixer. The mixed powders were then heated to 1823 K in graphite crucibles and held for 30 min to ensure uniformity (Ref. 21). Following this, liquid fluxes

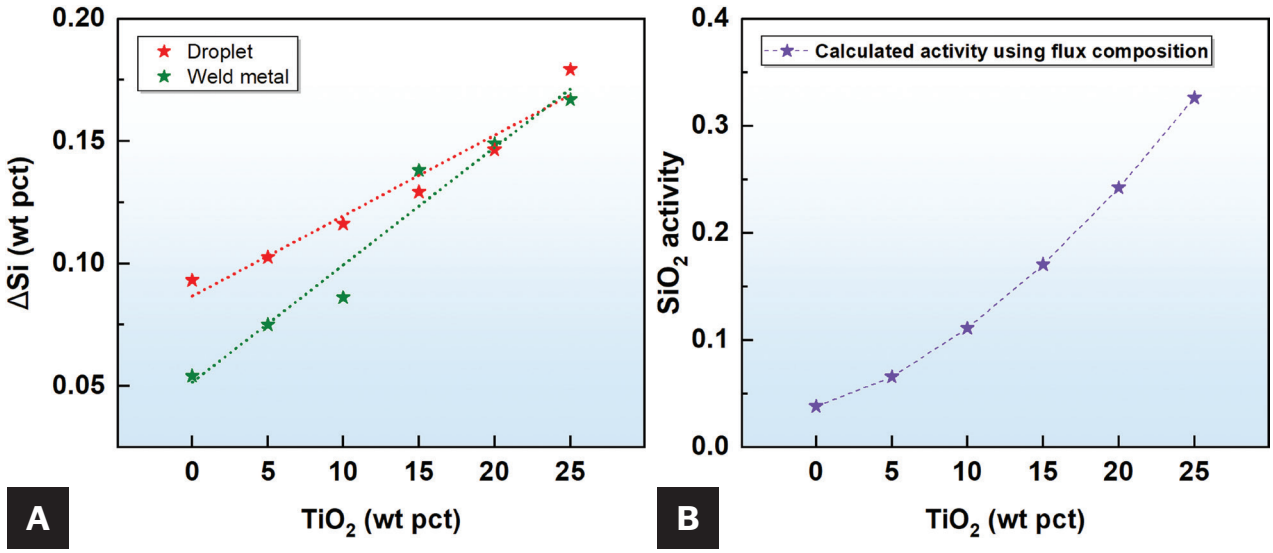

Fig. 2 — A — ΔSi value; B — SiO_2 activity as a function of TiO_2 content in CaO-SiO_2-MnO-TiO_2 fluxes.

Table 3 — Chemical Compositions of Employed Droplet and Weld Metal (wt-%)

Dilution Value		Droplet				Weld Metal			
		O	Mn	Si	Ti	O	Mn	Si	Ti
F-1	0.533	0.121	3.181	0.218	0	0.089	2.194	0.136	0.004
F-2	0.529	0.083	2.838	0.237	0.003	0.068	1.981	0.157	0.005
F-3	0.532	0.079	2.451	0.267	0.005	0.061	1.840	0.168	0.006
F-4	0.527	0.075	2.038	0.298	0.008	0.054	1.703	0.219	0.006
F-5	0.535	0.071	1.768	0.335	0.014	0.050	1.593	0.231	0.007
F-6	0.525	0.069	1.420	0.397	0.026	0.047	1.419	0.248	0.009

were rapidly cooled in water (273 K) (Ref. 22). The resulting fragmented fluxes were crushed and sized to 8–40 mesh (Ref. 23). Prior to welding, the fluxes underwent a 2-h baking at 973 K to eliminate residual graphite and moisture (Refs. 21, 24).

The SAW experiment was initially performed followed by the droplet collection experiment, in which droplets were intercepted during SAW. Both experimental setups employed a CHW-S3 (Atlantic, China) welding electrode, which was matched to high-strength low-alloy steel grades. In both experiments, the direct current electrode positive welding method was employed, with a current of 400 A and a voltage of 32 V. The SAW experiment utilized a surfacing welding method, utilizing EH36 grade shipbuilding steel plate as the BM. Before welding, the steel plate was polished using an angle grinder with 80-grit sandpaper to remove surface rust and defects. In the droplet collection experiment, a custom-made rapid cooling device was employed instead of the BM. At the same time, the electrode and flux compositions remained consistent with those used during SAW. Incorporating circulating cooling water markedly improved heat transfer efficiency, facilitating the rapid solidification of droplets and thereby ensuring effective capture. The droplet collection device was fabricated from pure copper, a heterogeneous material compared to iron. If the arc partially melted the copper plate and introduced contamination, any resulting Cu content in the droplets could be accurately identified and subtracted during compositional analysis. Moreover, pure copper ensured high thermal conductivity throughout the collection process. Solidified droplets were obtained by breaking the slag and then subjected to ultrasonic cleaning. Figure 1A shows the macroscopic appearance of the weld bead formed without a conventional weld pool during the droplet collection experiment. Due to rapid solidification, the slag wall solidified before collapsing, thereby preserving the

original morphology of the arc cavity in the form of a raised hollow structure. Figure 1B shows the collected droplets' typical size distribution, ranging from 4 to 8 mm.

Inductively coupled plasma optical emission spectrometry (PerkinElmer ICP-OES, Optima 8300 DV) was employed to analyze the metallic element contents of the BM, electrode, droplets, and WM. A LECO analyzer (LECO Corp. ONH836) determined the O contents. Three WM samples were sectioned, and a specimen was extracted from the center of each for compositional analysis. Additionally, three droplets were individually selected for separate compositional analysis. Tables 2 and 3 list the analyzed compositions of the BM, electrode, droplet, and WM, respectively. The calculation of the Δ values for droplets and WM is detailed in Equations A3 and A4 in the Appendix. Melting temperature and the activity of fluxes were calculated utilizing FactSage 8.1 software, employing FToxide and FactPS modules and pure liquid oxide as the standard reference state.

Results

The droplet zone pertains to the region where the electrode melts and forms droplets under the influence of arc plasma. The weld pool zone denotes the region affected by arc plasma and gases after the droplets merge into the weld pool. The slag-metal zone represents the region in contact with slag during the solidification process of the weld pool and is classified as a non-arc zone. Due to the extremely high temperatures and the catalytic effects of the arc plasma, the droplet zone, where the arc is situated, exerts a significantly stronger driving force for element transfer than other reaction zones in SAW (Refs. 25, 26). Elements decomposed from fluxes are initially transferred into droplets, with the possibility of being simultaneously transferred to the weld pool. Droplets are then diluted within the weld pool, and the final stage of element transfer is completed at the slag-metal interface. Element transfer behavior in the weld pool and slag-metal zones can be elucidated by comparing the changes in element composition between the droplets and the WM. If the Δ value of an element of droplets exceeds that of the WM, it indicates that the element is lost from the weld pool to slag following its transfer into droplets. Conversely, it suggests that the element transfers not only into droplets but also into the weld pool.

Figure 2A illustrates the ΔSi values of droplets and the WM as a function of TiO_2 content in the fluxes. ΔSi values of both droplets and the WM exhibited an upward trend with increasing TiO_2 content. Specifically, $\Delta_{Dr}Si$ values increased from 0.093 to 0.179 wt-%, while $\Delta_{WM}Si$ values increased from 0.054 to 0.167 wt-%. A positive ΔSi value indicated that Si in the fluxes was transferred to the droplet and the WM, with the extent of this transfer increasing progressively. Notably, despite the constant SiO_2 content across different flux groups, ΔSi values increased monotonically. The calculation results in Fig. 2B show that the SiO_2 activity in the fluxes increased with the increase of TiO_2 content. The transfer level of Si is proportional to the SiO_2 activity in the fluxes (Ref. 27). Zhang et al. (Ref. 28) proposed that adding TiO_2 could depolymerize SiO_2 network structures, thereby facilitating increased participation of Si in element transfer. In cases of

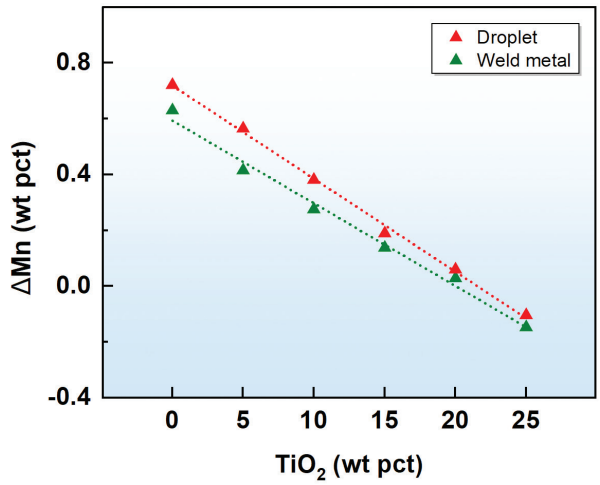

Fig. 3 — ΔMn value as a function of TiO_2 content in $CaO-SiO_2-MnO-TiO_2$ fluxes.

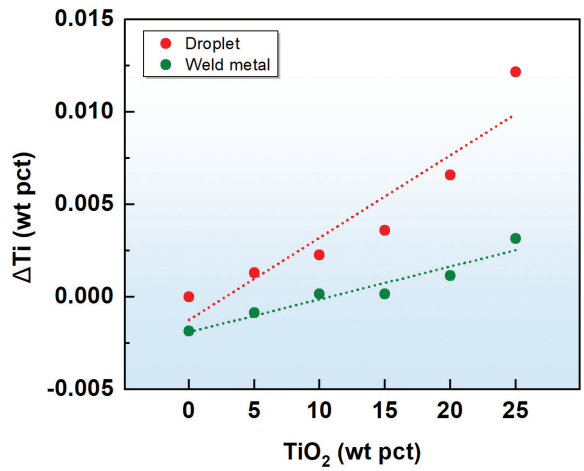

Fig. 4 — ΔTi value as a function of TiO_2 content in $CaO-SiO_2-MnO-TiO_2$ fluxes.

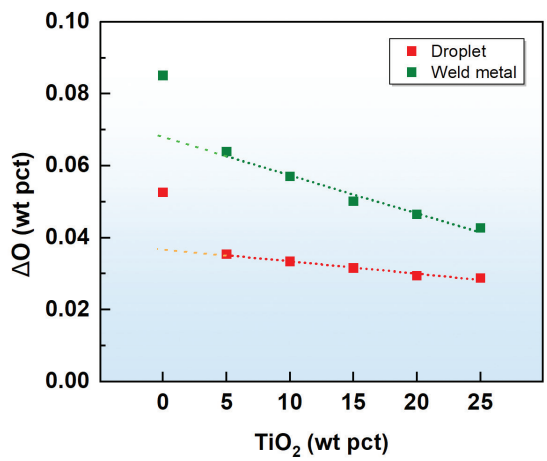

Fig. 5 — ΔO value as a function of TiO_2 content in $CaO-SiO_2-MnO-TiO_2$ fluxes.

Table 4 — Gas Components in Welding Estimated via the Gas-Slag-Metal Model (vol-%)

	CO	Mn	Fe	SiO	O	TiO_2	WM/Slag
F-1	9.521E-01	2.620E-02	5.159E-03	3.031E-03	5.713E-07	4.091E-09	3.51
F-2	9.548E-01	2.261E-02	5.190E-03	3.509E-03	5.844E-07	1.816E-07	3.65
F-3	9.574E-01	1.787E-02	5.232E-03	3.460E-03	6.715E-07	2.472E-07	3.76
F-4	9.592E-01	1.422E-02	5.264E-03	3.728E-03	7.353E-07	3.289E-07	3.85
F-5	9.611E-01	1.289E-02	5.274E-03	5.015E-03	6.581E-07	4.739E-07	3.83
F-6	9.624E-01	1.145E-02	5.284E-03	6.620E-03	5.927E-07	6.348E-07	3.91

identical flux composition, Δ_{Dr}Si values are basically greater than Δ_{WM}Si values, with the maximum difference reaching 0.039 wt-%. This indicated that Si loss in the weld pool and slag-metal zone reached 0.039 wt-%.

Figure 3 presents the ΔMn values of droplets and the WM as a function of TiO_2 content in the fluxes. The ΔMn values of droplets and the WM both decreased as TiO_2 replaced MnO, with Δ_{Dr}Mn values decreasing from 0.720 to −0.104 wt-% and Δ_{WM}Mn values decreasing from 0.629 to −0.147 wt-%. Negative ΔMn values indicate a net reduction in Mn content. When the flux composition is identical, Δ_{Dr}Mn values are higher than Δ_{WM}Mn values, with the maximum difference reaching 0.149 wt-%. This suggests that Mn loss in the weld pool and slag-metal zone extended to 0.149 wt-%. When the TiO_2 content exceeded 21.05 wt-%, droplets and the WM exhibited a Mn net loss. The onset of Mn loss occurred in the droplet zone, likely attributable to the volatilization of Mn at elevated temperatures (Ref. 29).

Figure 4 depicts the ΔTi values of droplets and the WM as a function of TiO_2 content in the fluxes. The ΔTi values of droplets and the WM increased with the increase in TiO_2 content. Specifically, Δ_{Dr}Ti values increased from 0 to 0.012 wt-%, and Δ_{WM}Ti values increased from −0.002 to 0.003 wt-%. Negative ΔTi values indicate a net reduction in Ti content. Δ_{Dr}Ti values were consistently positive and exceeded Δ_{WM}Ti values, which varied from negative to positive, exhibiting a maximum disparity of 0.009 wt-%. This demonstrated that Ti loss in the weld pool and slag-metal zone amounted to 0.009 wt-%.

Figure 5 demonstrates the ΔO values of the droplets and the WM as a function of TiO_2 content in the fluxes. The ΔO values of both the droplets and WM decreased as MnO was replaced by TiO_2, with Δ_{Dr}O values decreasing from 0.053 to 0.029 wt-% and Δ_{WM}O values decreasing from 0.085 to 0.043 wt-%. Specifically, as the TiO_2 content in the fluxes increased from 0 to 5 wt-%, the transfer levels of O decreased markedly, indicating that the addition of TiO_2 diminished the O potential of the fluxes. During SAW, O consistently transferred to the droplets and WM, as evidenced by the positive ΔO values. When the flux composition remained the same, the Δ_{WM}O values exceed the Δ_{Dr}O values, with a peak difference of 0.032 wt-%.

Discussion

During SAW, the fluxes provide an effective shielding environment that prevents atmospheric gases from interacting with the WM. Consequently, the composition of the WM is solely determined by contributions from the electrode, BM, and fluxes (Ref. 30). In this study, the variations in droplet and WM compositions among different experimental groups were attributed to differences in flux composition. As previously noted, although the SiO_2 content in the fluxes remained constant, the increase in TiO_2 content could induce depolymerization of the SiO_2 network, thereby enhancing the transfer of Si. MnO served as the sole source of Mn in the system, and the observed decrease in Mn content in both the droplet and WM was attributed to the progressive substitution of MnO by TiO_2 in the fluxes. As expected, adding TiO_2 significantly increased the partial pressure of the TiO_2 gas, thereby promoting the transfer of Ti. Moreover, the replacement of oxides with higher O potential (such as MnO) by those with lower O potential (such as TiO_2) led to a reduction in the overall O potential of the fluxes, which in turn resulted in lower O content in both the droplet and the WM.

Alloying Element Transfer

As mentioned above, the element transfer behaviors of Si, Mn, and Ti exhibit similar trends. Specifically, the transfer levels of Si and metallic elements (hereafter referred to as alloying elements) from fluxes to droplets are higher than those to the WM, indicating that the Δ_{Dr}M value exceeds the Δ_{WM}M value. This suggests that elements originating from fluxes are further depleted in the subsequent weld pool zone or slag-metal zone after their initial transfer to the droplets. The behavior of Ti transfer is particularly notable. In this study, the absence of Ti in the electrode implies that the fluxes served as the sole source of Ti before droplets descended into the weld pool. When the TiO_2 content was below 9.78 wt-%, the Δ_{Dr}Ti value was positive, signaling transfer to the droplets, whereas the Δ_{WM}Ti value was negative, reflecting Ti depletion. Therefore, the primary location of alloying element transfer during SAW was concentrated within the droplet zone.

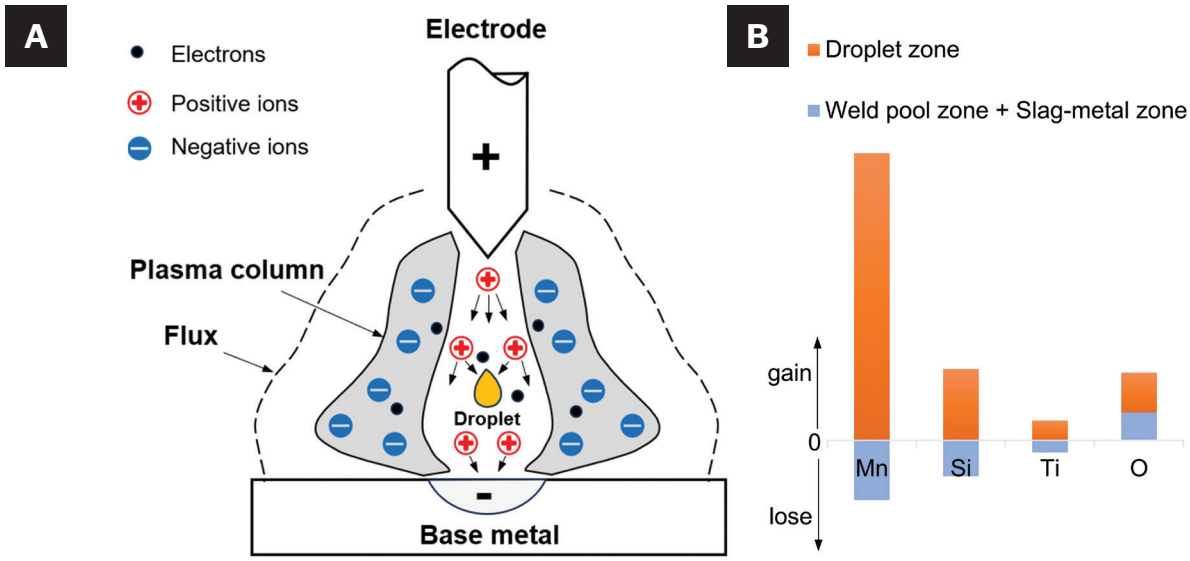

Fig. 6 — Schematic representation of: A — Arc column distributions; B — element transfer locations during SAW.

The similarity in transfer behavior among alloying elements may be attributed to their comparable valence electron configurations, which were less than or equal to half the maximum capacity (i.e., 4) of the outermost shell. This is exemplified by Mn, which possesses a first ionization energy of 717.3 kJ/mol. This results in a weaker binding affinity for outer-shell electrons, leading to lower first ionization energies than non-metallic elements with more than four valence electrons, such as O, which exhibits a first ionization energy of 1313.9 kJ/mol. Therefore, alloying elements are more readily ionized within the arc column and exhibit a greater tendency to transfer into droplets under arc column conditions. The loss of alloying elements is likely attributed to oxidation in the weld pool. The oxides in the molten steel are driven by cavity bridge forces to coalesce, forming large-sized inclusions (Ref. 31). Li et al. (Ref. 32) suggested that larger inclusions were more prone to inducing channel segregation through flotation, resulting in the depletion of alloying elements. Tian et al. (Ref. 33) identified the presence of FeO in the slag following welding, thereby confirming the capacity of the oxide to transfer from the weld pool into the slag phase. Consequently, the loss of alloying elements can be attributed to the flotation of inclusions formed by metal oxides within the molten steel.

Table 4 presents the estimated welding atmosphere at 2273 K, calculated using the "gas-slag-metal" model based on FactSage 8.1 software (Ref. 27). In this context, WM/Slag represents the mass ratio of weld metal to slag. These results further elucidate the influence of flux composition variations on the chemical composition of both the droplets and the WM. The gas species beneath the slag layer primarily included CO, CO_2, Mn, Fe, SiO, FeO, Ca, O, O_2, and TiO_2. Among the gaseous species, Mn vapor pressure was the only one that decreased with the reduction of MnO content. In contrast, partial pressures of other oxide gases increased with rising TiO_2 content. Notably, the partial pressure of SiO increased with increasing TiO_2 content, mirroring the trend observed in the activity of SiO_2. A comparison between F-1 and F-2 revealed a significant increase in the partial pressure of TiO_2 gas, indicating that variations in flux composition can markedly alter the welding atmosphere and, thereby, influence the transfer behavior of alloying elements. Interestingly, an increase in the partial pressure of atomic O was also observed, which may have resulted from the thermal decomposition of SiO_2. However, this elevated O partial pressure did not appear to enhance the O uptake of the WM and the droplets. This may be attributed to the preferential oxidation of metallic vapors such as Mn and Fe before their incorporation into the droplet.

O Transfer

Figure 6 presents a schematic representation of arc column distributions and element transfer locations during SAW. As noted previously, the contribution of droplets to the O transfer level was lower than the total O content acquired by the WM during SAW (i.e., $\Delta_{WM}O$ values exceeded $\Delta_{Dr}O$ values). This suggests that, in addition to droplets, alternative sources contributed to the increase in O content in the WM. As discussed regarding the loss of alloying elements, alloying elements likely exited the weld pool as oxides at the slag-metal interface. Therefore, the likelihood of O being supplied via reactions at the slag-metal interface is limited, and the transfer of excess O was more likely to originate from the plasma-weld pool interface, as shown in Fig. 6A. The disparity in transfer positions between O and alloying elements primarily arises from variations in their masses and ionization mechanisms (Ref. 34). Under the influence of the arc, alloying elements are directly ionized into positive ions and electrons (Ref. 35). However, the formation of O plasma occurs through two mechanisms: in the center of the arc, O atoms are ionized into positive ions and electrons (Refs. 36, 37), and at the periphery of the arc, electrons attach to low-energy O particles, forming negative ions (Ref. 38). Therefore, the transfer of O must be considered from the perspectives of both positive and negative ions. On the one hand, in addition to transferring to droplets, O^+ and metal ions are also attracted by the electrode and move to

the weld pool. However, due to the mass difference between the two, the velocity of O^+ is significantly higher than that of metal ions, facilitating its movement to the weld pool. Thus, the transfer levels of O^+ within the weld pool zone exceed those of metal ions. On the other hand, O^{2-} ions at the edge of the arc can engage in electrochemical reactions within the weld pool, leading to their transfer into the weld pool (Ref. 13). In summary, as illustrated in Fig. 6B, most alloying element transfer and a portion of O transfer occur within the droplet zone, while alloying element loss and the remaining O transfer occur in the weld pool and slag-metal zones.

Conclusions

This study conducted droplet collection experiments and SAW using CaO-SiO_2-MnO-TiO_2 fluxes. The transfer levels of Si, Mn, Ti, and O from fluxes into droplets and, finally, into the WM were quantified and compared, facilitating the determination of the specific locations of element transfer. The main conclusions can be summarized as follows:

1. The transfer levels of Si, Mn, and Ti to droplets were higher than those to the WM, indicating that the alloying elements primarily transfered in the droplet zone, with the loss of alloying elements occurring mainly after the droplets fell into the weld pool.

2. The transfer levels of O to droplets were lower than those to the WM, indicating that O continued to transfer in the weld pool zone even after its initial transfer in the droplet zone.

Acknowledgments

The authors sincerely acknowledge the financial support from the National Natural Science Foundation of China (Grant Nos. W2411047 and 52404393), the National Key R&D Program of China (Grant No. 2023YFB3709900), and the Fundamental Research Funds for the Central Universities (Grant Nos. N2402016 and N25GFZ018).

Disclosure Statement

On behalf of all authors, the corresponding author states that there is no conflict of interest.

References

1. Zhang, Y., Zhang, J., Liu, H., Wang, Z., and Wang, C. 2022. Addressing weld metal compositional variations in EH36 shipbuilding steel processed by CaF_2-SiO_2-CaO-TiO_2 fluxes. *Metallurgical and Materials Transactions B* 53(3): 1329–1334. DOI: 10.1007/s11663-022-02480-y

2. Shen, Y., Gu, Z., and Wang, C. 2024. Phase transformation behaviors in the heat-affected zones of ferritic heat-resistant steels enabled by in situ CSLM observation. *Acta Metallurgica Sinica* 60(6): 802–816. DOI: 10.11900/0412.1961.2023.00045

3. Wang, C., and Zhang, J. 2021. Fine-tuning weld metal compositions via flux optimization in submerged arc welding: An overview. *Acta Metallurgica Sinica* 57(9): 1126–1140. DOI: 10.11900/0412.1961.2021.00148

4. Bai, H., Zhang, Y., Zhao, Y., Zhong, M., Li, Z., and Wang, C. 2025. Numerical analysis of slag viscosity effects mechanism in submerged arc welding pool. *Metallurgical and Materials Transactions B* 56(2): 1659–1671. DOI: 10.1007/s11663-025-03448-4

5. Yuan, H., Zhang, Y., Liu, H., Li, Z., and Wang, C. 2025. Bond characteristic-dependent viscosity variations in CaF_2-SiO_2-Al_2O_3-MgO welding fluxes. *Welding Journal* 104(4): 107-s to 118-s. DOI: 10.29391/2025.104.009

6. Delagnes, D., Lamesle, P., Mathon, M. H., Mebarki, N., and Levaillant, C. 2005. Influence of silicon content on the precipitation of secondary carbides and fatigue properties of a 5% Cr tempered martensitic steel. *Materials Science and Engineering A* 394(1–2): 435–444. DOI: 10.1016/j.msea.2004.11.050

7. Yuan, H., Zhang, Y., and Wang, C. 2025. Influence of MnO upon electrical conductive mechanisms of submerged arc welding fluxes: Insights from ab initio molecular dynamics simulations. *Acta Metallurgica Sinica*. DOI: 10.11900/0412.1961.2025.00065

8. Wu, Y., Yuan, X., Zhong, M., Ma, J., Kaldre, I., and Wang, C. 2024. Penetration-dependent microstructures in TiO_2-induced weld metal of EH36 shipbuilding steel. *Metallurgical and Materials Transactions A* 55(5): 1295–1301. DOI: 10.1007/s11661-024-07336-5

9. Pandey, N. D., Bharti, A., and Gupta, S. R. 1994. Effect of submerged arc welding parameters and fluxes on element transfer behaviour and weld-metal chemistry. *Journal of Materials Processing Technology* 40(1): 195–211. DOI: 10.1016/0924-0136(94)90486-3

10. Singh, K., and Pandey, S. 2009. Recycling of slag to act as a flux in submerged arc welding. *Resources, Conservation and Recycling* 53(10): 552–558. DOI: 10.1016/j.resconrec.2009.04.006

11. Mitra, U., and Eagar, T. W. 1991. Slag-metal reactions during welding. Part II. Theory. *Metallurgical Transactions B* 22(1): 73–81. DOI: 10.1007/BF02672529

12. Zhang, J., Coetsee, T., and Wang, C. 2020. Element transfer behaviors of fused CaF_2-SiO_2 fluxes subject to high heat input submerged arc welding. *Metallurgical and Materials Transactions B* 51(1): 16–21. DOI: 10.1007/s11663-019-01753-3

13. Kim, J., Frost, R., Olson, D., and Blander, M. 1990. Effect of electrochemical reactions on submerged arc weld metal compositions. *Welding Journal* 69(12): 446-s to 453-s.

14. Murphy, A. B. 2001. Thermal plasmas in gas mixtures. *Journal of Physics D: Applied Physics* 34(20): R151. DOI: 10.1088/0022-3727/34/20/201

15. Sengupta, V., Havrylov, D., and Mendez, P. F. 2019. Physical phenomena in the weld zone of submerged arc welding – A review. *Welding Journal* 98(10): 283-s to 313-s. DOI: 10.29391/2019.98.025

16.Mitra, U., and Eagar, T. W. 1991. Slag-metal reactions during welding. Part I. Evaluation and reassessment of existing theories. *Metallurgical Transactions B* 22(1): 65–71. DOI: 10.1007/BF02672528

17. Wang, G., Zhang, Y., Zhao, Y., Bai, H., Kaldre, I., and Wang, C. 2024. Unveiling droplet zone element transfer behaviors of CaO-SiO_2-MnO fluxes in the EH36 shipbuilding steel subject to submerged arc welding. *Metallurgical and Materials Transactions B* 55(6): 4216–4222. DOI: 10.1007/s11663-024-03231-x

18. Tathgir, S., and Bhattacharya, A. 2016. Activated-TIG welding of different steels: Influence of various flux and shielding gas. *Materials and Manufacturing Processes* 31(3): 335–342. DOI: 10.1080/10426914.2015.1037914

19. Natalie, C. A., Olson, D. L., and Blander, M. 1986. Physical and chemical behavior of welding fluxes. *Annual Review of Materials Science* 16(1): 389–413. DOI: 10.1146/annurev.ms.16.080186.002133

20. Singh, B., Khan, Z. A., Siddiquee, A. N., and Maheshwari, S. 2016. Effect of CaF_2, FeMn and NiO additions on impact strength and hardness in submerged arc welding using developed agglomerated fluxes. *Journal of Alloys and Compounds* 667: 158–169. DOI: 10.1016/j.jallcom.2016.01.133

21. Indacochea, J. E., Blander, M., Christensen, N., and Olson, D. L. 1985. Chemical reactions during submerged arc welding with FeO-MnO-SiO_2 fluxes. *Metallurgical Transactions B* 16(2): 237–245. DOI: 10.1007/BF02679715

22. Yuan, H., Zhang, Y., Zhao, Y., Li, J., Li, Z., and Wang, C. 2025. Structural role of CaF_2 upon welding flux viscosity. *Welding Journal* 104(5): 164-s to 174-s. DOI: 10.29391/2025.104.013

23. Zhang, Y., Liu, H., Coetsee, T., Wang, Z., and Wang, C. 2023. Identifying oxygen transfer pathways during high heat input submerged arc welding: A case study into CaF_2-SiO_2-CaO-TiO_2 fluxes. *Metallurgical and Materials Transactions B* 54(6): 2875–2880. DOI: 10.1007/s11663-023-02922-1

24. Liu, H., Zhang, Y., Zhong, M., Feng, Y., Liu, J., and Wang, C. 2024. Exploring Cr and O transfer mechanisms in the weld metal of P92 heat-resistant steel processed by CaF_2-Cr_2O_3 fluxes. *Metallurgical and Materials Transactions B* 55(1): 8–13. DOI: 10.1007/s11663-023-02951-w

25. Zheng, J., Sun, B., Yang, R., Song, X., Li, X., and Pu, Y. 2008. Metal Al produced by H2 plasma reduction of $AlCl_3$: A thermodynamic and kinetic study on the plasma chemistry. *Journal of Physical Chemistry* B 112(40): 12748–12752. DOI: 10.1021/jp8035204

26. Debek, R., Azzolina-Jury, F., Travert, A., and Mauge, F. 2019. A review on plasma-catalytic methanation of carbon dioxide – looking for an efficient catalyst. *Renewable & Sustainable Energy Reviews* 116: 109427. DOI: 10.1016/j.rser.2019.109427

27. Zhang, J., Wang, C., and Coetsee, T. 2021. Thermodynamic evaluation of element transfer behaviors for fused CaO-SiO_2-MnO fluxes subjected to high heat input submerged arc welding. *Metallurgical and Materials Transactions B* 52(4): 1937–1944. DOI: 10.1007/s11663-021-02221-7

28. Zhang, Y., Yuan, H., Tian, H., Wang, Z., and Wang, C. 2023. Elucidating electrical conductive mechanisms for CaF_2-SiO_2-CaO-Ti_2welding fluxes. *Metallurgical and Materials Transactions B* 54(6): 3023–3030. DOI: 10.1007/s11663-023-02885-3

29. Chu, J., Bao, Y., Li, X., Wang, M., and Gao, F. 2021. Kinetic study of Mn vacuum evaporation from Mn steel melts. *Separation and Purification Technology* 255: 117698. DOI: 10.1016/j.seppur.2020.117698

30. Lau, T., Weatherly, G., and McLean, A. 1985. The sources of oxygen and nitrogen contamination in submerged arc welding using CaO-Al_2O_3 based fluxes. *Welding Journal* 64(12): 343-s to 347-s.

31. Wang, J., Zhang, L., Zhang, Y., Ren, Q., and Duan, H. 2021. Effect of diameter and contact angle on initial aggregation of solid inclusions in molten steels. *Metallurgical and Materials Transactions B* 52(5): 2831–2836. DOI: 10.1007/s11663-021-02284-6

32. Li, D., Chen, X., Fu, P., Ma, X., Liu, H., Chen, Y., Cao, Y., Luan, Y., and Li, Y. 2014. Inclusion flotation-driven channel segregation in solidifying steels. *Nature Communications* 5: 5572. DOI: 10.1038/ncomms6572

33. Tian, H., Zhang, Y., Shi, S., Wang, G., and Wang, C. 2024. Recycling welding fluxes: A case study into manganese-silicate system. *Metallurgical and Materials Transactions B* 55(6): 4398–4407. DOI: 10.1007/s11663-024-03252-6

34. Jenett, H., Ai, X. T., Hodoroaba, V. D., Iga, I., and Tao, L. M. 1999. Low-energy BO and BO_2 emission from H_2BO_3 sputtered in a low-pressure high-frequency SNMS plasma. *Nuclear Instruments & Methods in Physics Research Section B* 155(1–2): 13–24. DOI: 10.1016/S0168-583X(99)00291-8

35. Zielinska, S., Pellerin, S., Dzierzega, K., Valensi, F., Musiol, K., and Briand, F. 2010. Measurement of atomic Stark parameters of many Mn I and Fe I spectral lines using GMAW process. J*ournal of Physics D: Applied Physics* 43(43): 434005. DOI: 10.1088/0022-3727/43/43/434005

36. Keika, K., Kistler, L.M., and Brandt, P.C. 2013. Energization of O^+ ions in the Earth's inner magnetosphere and the effects on ring current buildup: A review of previous observations and possible mechanisms. *Journal of Geophysical Research – Space Physics* 118(7): 4441–4464. DOI: 10.1002/jgra.50371

37. Lim, Y. D., Lee, S. H., Yoo, W. J., Jung, O.J., Kim, S. C., and Lee, H. C. 2009. Roles of F and O radicals and positive ions in a SF_6/O_2 plasma in forming deep via structures. *Journal of the Korean Physical Society* 54(5): 1774–1778. DOI: 10.3938/jkps.54.1774

38. Cao, L., Ma, X., Deng, L., Lu, M., and Xin, Y. 2021. Axial diagnosis of radio-frequency capacitively coupled Ar/O_2 plasma. *Acta Physica Sinica* 70(11): 115204. DOI: 10.7498/aps.70.20202113

Appendix: Computation of Δ Value for WM and Droplets

The dilution effect of electrode and BM on WM composition can be quantified by calculating the nominal composition, as demonstrated in Equation A1 (Ref. 3).

$$M_N = M_{BM} \times d + M_{El} \times (1 - d) \quad \text{(A1)}$$

where M_N represents the nominal composition of the WM, M_{BM} denotes the BM composition, M_{El} represents the electrode composition, and d is the dilution value. The dilution value, which represents the dilution effect of BM on droplets, can be determined by analyzing the macroscopic morphology of the WM, as detailed in Equation A2

$$d = A_1 / A_2 \quad \text{(A2)}$$

where A_1 represents the area of diluted BM and A_2 denotes the total area of the WM.

To quantify the total contribution of the fluxes to element transfer throughout the entire SAW, the Δ value parameter is employed for evaluation, as follows in Equation A3

$$\Delta_{WM} = M_{WM} - M_N \quad \text{(A3)}$$

where M_{WM} indicates the measured composition of the WM. A positive Δ_{WM} value signifies the elements transfer from fluxes to the WM, whereas a negative Δ_{WM} value indicates the loss of elements from the WM to slag.

To quantify the contribution of element transfer behavior in the droplet zone to the overall SAW, it is essential to account for the dilution effect of droplets by the BM. The parameter Δ_{Dr} represents the change in droplet composition after dilution, as follows in Equation A4

$$\Delta_{Dr} = (M_{Dr} - M_{El}) \times (1 - d) \quad \text{(A4)}$$

where M_{Dr} denotes the droplet composition, and a positive Δ_{Dr} value signifies that elements transfer from plasma to droplets, whereas a negative Δ_{Dr} value indicates that elements are lost from droplets to plasma. This calculation method effectively eliminates the influence of volume discrepancies between droplets and the WM, allowing for a direct comparison of the contribution of fluxes to element transfer in droplets and the WM based solely on compositional analysis.

GUANYI WANG, **YANYUN ZHANG**, **HUIYU TIAN**, and **CONG WANG** (*wangc@smm.neu.edu.cn*) are with the Key Laboratory for Ecological Metallurgy of Multimetallic Mineral (Ministry of Education), School of Metallurgy, Northeastern University, Shenyang, China. **ZUSHU LI** is with WMG, University of Warwick, Coventry, United Kingdom.